Macromolecules

Open Access

This article is licensed under CC-BY 4.0

pubs.acs.org/Macromolecules

Article

Phase-Separation Pathway Selection in PNIPAM via End-Group Ionisation and NaCl Salting-Out

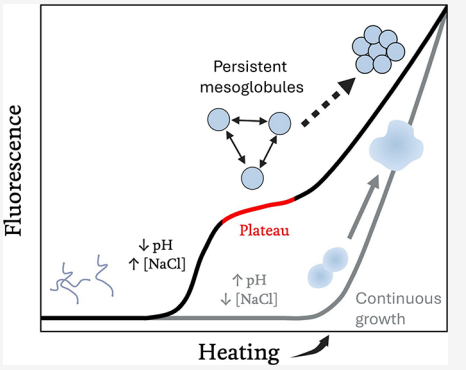
Yuhang Zhang, Tianlai Xia, Jin Qin, Thieme T. Schmidt, Rachel K. O'Reilly, Ulrich F. Keyser,* and Jeremy J. Baumberg*

Cite This: https://doi.org/10.1021/acs.macromol.6c01188

Read Online

ACCESS | Metrics & More | Article Recommendations | Supporting Information

ABSTRACT: Nile Red fluorescence reveals three distinct phase-separation pathways in heterotelechelic HS−PNIPAM−COOH: multistage, monotonic, and suppressed transitions. Aqueous HS−PNIPAM−COOH ($M_n \approx 6$ kDa) is investigated over pH 3−10 and at NaCl concentrations from 0 to 1.0 M using fluorescence, turbidimetry, dynamic light scattering, and temperature-controlled single-particle tracking. Multistage transitions, comprising an initial fluorescence rise, an intermediate plateau, and a second rise, occur under weakly ionised, high-salt conditions. Intermediate conditions produce a monotonic fluorescence increase, whereas strongly ionised, weakly screened conditions suppress detectable phase separation. The multistage sample, citrate buffer containing 1.0 M NaCl, forms stable, micrometre-scale PNIPAM-rich droplets with no further growth across the fluorescence plateau despite increasing turbidity. Growth resumes only above the plateau. By contrast, the representative monotonic samples (citrate buffer without added NaCl and borate buffer containing 1.0 M NaCl) show continuous droplet growth during the temperature holds. On cooling from 60 to 40 °C, multistage droplets remain nearly unchanged in size before undergoing delayed, rapid, collective dissolution at lower temperature, whereas monotonic droplets shrink progressively before later rapid dissolution. These results show that pH and NaCl concentration control both the phase-separation pathway and mesoglobule persistence, producing different high-temperature states that rehydrate differently on cooling.



1. INTRODUCTION

The thermoresponsive coil-to-globule transition of poly(*N*-isopropylacrylamide) (PNIPAM) and its subsequent phase separation are central to responsive soft-material design.[1] On heating through its lower critical solution temperature (LCST) in water, PNIPAM chains partially dehydrate and collapse from hydrated coils into compact globules.[2] At sufficient concentration, these globules associate into larger clusters that may grow continuously or persist as relatively monodisperse, colloidally stable mesoglobules.[3−5] Controlling mesoglobule formation and persistence is important for applications ranging from gene delivery, where mesoglobules can serve as colloidal carriers,[6] to PNIPAM-based 3D printing, where rapid phase separation and precipitation are required.[7]

Mesoglobule stability depends strongly on interfacial dynamics. Nonradiative energy transfer and fluorescence-depolarisation measurements showed that PNIPAM mesoglobules formed just above the demixing temperature are initially fluid-like and capable of merging but become rigid and nonmerging within a further 6 °C of heating.[8] Small-angle neutron scattering (SANS) measurements performed under pressure show that, under strongly dehydrating conditions, collapsed PNIPAM globules initially grow by diffusion-limited coalescence into fractal-like clusters but then develop a dense polymer-rich shell at the mesoglobule surface that impedes chain interpenetration and arrests further coalescence.[9−11] Under less dehydrating conditions, no such shell forms, and mesoglobules instead grow by unhindered diffusion-limited coalescence. Pressure-jump experiments also identified two dissolution modes: under weak driving forces, mesoglobules shrank primarily by the release of individual chains from the surface, whereas under stronger osmotic driving forces, water swelled the mesoglobule interior first, loosening chain association and accelerating disintegration.[12] Although these studies used pressure rather than temperature as the control variable, they suggest that mesoglobule formation, arrest, and dissolution are governed by how rapidly dehydration proceeds relative to the timescale of interfacial relaxation and chain rearrangement.

Received: April 29, 2026
Revised: October 10, 2026
Accepted: October 12, 2026

Downloaded from pubs.acs.org/macmobx/article-pdf/doi/10.1021/acs.macromol.6c01188/6895793939/ma-2026-011886.pdf by UNIV OF CAMBRIDGE user on 23 October 2026

© XXXX The Author(s). Published by American Chemical Society

Here we explore whether the same dynamics can be accessed by tuning solution variables. Previous work shows that NaCl can both screen electrostatic repulsion and enhance PNIPAM dehydration. NMR measurements indicate that NaCl lowers the energetic cost of hydrophobic contact formation during early chain collapse,[13] and measurements of Hofmeister-ion effects showed that NaCl depresses the LCST primarily by increasing the surface-tension penalty around hydrophobically hydrated moieties.[14] Increasing the NaCl concentration may therefore accelerate dehydration and favour an arrested mesoglobule state. End-group ionisation provides another control, particularly for low-molecular-weight PNIPAM, where the termini contribute substantially to the overall polymer character.[15−17] Carboxyl-terminated PNIPAM stars, for example, remain unimeric above the LCST when their termini are strongly deprotonated but aggregate readily at lower pH or after salt addition.[18] Ionisation also alters local hydration: carboxylates are strongly hydrated,[19] and carboxylic-acid-containing PNIPAM copolymers show pH-dependent thermal responses.[20,21] Thus, pH and NaCl may jointly control electrostatic repulsion, terminal-group hydration, and the rate of interfacial dehydration.

Resolving this interplay requires measurements spanning several structural scales. Nile Red reports changes in the local polymer-rich microenvironment because its fluorescence is weak in aqueous PNIPAM solutions below the LCST but rises sharply above the transition as the dye partitions into hydrophobic polymer-rich domains.[22] Turbidimetry detects larger, optically distinct structures; dynamic light scattering (DLS) reports ensemble relaxation dynamics; and single-particle tracking directly resolves droplet-scale growth and dissolution. Combining these probes allows local dehydration to be related to the emergence, evolution, and persistence of mesoscopic PNIPAM-rich assemblies.

In this work, heterotelechelic HS−PNIPAM−COOH ($M_n \approx$ 6 kDa) serves as a model system with two ionisable termini: the carboxyl group becomes increasingly deprotonated as pH rises,[23] whereas the aliphatic thiol can ionise at alkaline pH.[24] By varying the pH from 3 to 10 and the NaCl concentration from 0 to 1.0 M over repeated thermal cycles, we identify three distinct phase-separation behaviours: (i) multistage transitions with long-lived mesoglobule intermediates, (ii) monotonic transitions, and (iii) effective suppression of interchain association. We show that rapid heating into the fluorescence-plateau region generates micrometre-scale mesoglobules that form close to their final size and remain stable throughout the temperature hold. The fluorescence profile therefore provides an operational map for selecting conditions that produce either stable mesoglobule populations or continuously growing clusters, offering a practical route to control cluster size and kinetic stability through solution pH, NaCl concentration, and temperature.

2. METHODS

2.1. Materials and Sample Preparation

Heterotelechelic HS−PNIPAM−COOH (M_n = 6 kDa; reported M_w/M_n = 1.2; Sigma-Aldrich) was dissolved in water at 1 mM. SEC gave a PMMA-calibrated M_n of 3.3 kDa and a dispersity of M_w/M_n = 1.12; the supplier value of 6 kDa is used throughout (Supporting Information, Section S1). Before use, the polymer was treated with 10 mM tris(2-carboxyethyl)phosphine (TCEP; Invitrogen) at pH 7.4 and 25 °C for 30 min to reduce disulfides formed during storage.[25,26] TCEP itself did not measurably change the phase transition of a thiol-free PNIPAM−COOH control across repeated thermal cycles, whereas removing TCEP altered the HS−PNIPAM−COOH response, consistent with disulfide formation (Section S2 and Figure S6). Purification by precipitation preserved the pathway assignments, with heating onsets within 0.8 °C of those of the as-received polymer. The concentration-dependent cloud point in pure water is also reported in Section S1.

For each measurement, 25 μL of reduced polymer stock was added to 1 mL of 10 mM citrate (J61391.AK; pH 3.0), Tris (J60636.K2; pH 7.4), or borate (J62154.AK; pH 10.0) buffer (Thermo Scientific); pH values were adjusted and measured at 25 °C. This leads to a final 0.15 mg mL^{-1} PNIPAM and around 0.244 mM TCEP concentration. NaCl was added to final concentrations of 0, 0.1, 0.5, or 1.0 M. A 10 mM MOPS buffer (J61843.AP) was also included because its pK_a has a smaller absolute temperature coefficient than that of Tris ($\Delta pK_a/\Delta T \approx -0.011$ °C^{-1} compared with −0.028 °C^{-1}); the MOPS measurements and the estimated pH−temperature profiles of all buffers are given in Section S3. Samples and polymer-free blanks were prepared in ultrapure water and filtered through 0.22 μm Millex PES filters. Buffer concentrations were limited to 10 mM to reduce ionic-strength and specific-ion effects.[27−29] For the extended pH series at 1.0 M NaCl, samples were prepared similarly at pH 5.5−7.0 in 10 mM MES buffer (J61587.AP) and at pH 4.5 in 10 mM citrate buffer (Section S6).

2.2. Nile Red Fluorescence

Nile Red (Sigma-Aldrich) was dissolved in DMSO at 1 mg mL^{-1} and added to each sample at a final concentration of 7.8 μM; dye-concentration controls are provided in Section S4. Fluorescence was recorded in Hellma cuvettes using a Cary Eclipse fluorometer (λ_{ex} = 543 nm; λ_{em} = 650 nm). Samples underwent four heating−cooling cycles from 10 to 60 °C at 1 °C min^{-1}. Signals from matched polymer-free blanks were subtracted (Figure S8a).

2.3. Turbidimetry and Differential Scanning Calorimetry

Turbidity was measured as the apparent absorbance at 550 nm (A_{550}) using a Cary 300 Bio spectrophotometer. Dye-free polymer samples in BRAND semi-micro cuvettes were measured against matched buffer blanks during four heating−cooling cycles from 10 to 60 °C at 1 °C min^{-1}. Photographs were taken at 30, 40, 50, and 60 °C during heating at the same rate (Figure S12).

Solution status differential scanning calorimetry was performed on four representative samples (citrate with 1.0 M NaCl, citrate without added NaCl, Tris with 1.0 M NaCl, and Tris without added NaCl) using a TA Instruments NanoDSC as an independent, label-free probe of the thermal transition (Section S8). Heating and cooling ramps were performed at 1 °C min^{-1} under a constant pressure of 3 atm, and the signal from a matched solvent blank was subtracted.

2.4. Dynamic Light Scattering and Zeta-Potential Measurements

For DLS, 200 μL aliquots were loaded into BRAND UV microcuvettes and measured using a Malvern Zetasizer Nano ZSP in 173° backscatter mode. Samples equilibrated at room temperature were transferred to the instrument, which had been preset to the target temperature. Thirty consecutive 30 s acquisitions were recorded without further equilibration, with 10 s between acquisitions. Because the turbid, evolving samples were susceptible to multiple scattering, collective flow, and sedimentation-driven number fluctuations, instrument-reported size distributions were not used. Analysis was restricted to the intensity autocorrelation function, $g^{(2)}(\tau) - 1$ (Section S10). Previous studies show that mesoglobule formation produces an approximately single-exponential correlation decay, consistent with a relatively monodisperse population, whereas floc formation produces a stretched decay associated with a broader, polydisperse population.[30]

Downloaded from pubs.acs.org/macmobx/article-pdf/doi/10.1021/acs.macromol.6c01188/6895939/ma-2026-011886.pdf by UNIV OF CAMBRIDGE user on 23 October 2026

https://doi.org/10.1021/acs.macromol.6c01188
Macromolecules XXXX, XXX, XXX−XXX

Zeta potentials were measured in triplicate at 25 °C using the same instrument and folded capillary cells (DTS1070). Samples were equilibrated for 120 s, and zeta potentials were calculated from electrophoretic mobilities using the Smoluchowski approximation.

2.5. Optical Microscopy and Single-Particle Tracking

Three representative samples were examined by temperature-controlled dark-field microscopy during isothermal holds following heating and stepwise cooling: citrate without added NaCl (C0; monotonic), citrate containing 1.0 M NaCl (C1; multistage), and borate containing 1.0 M NaCl (B1; monotonic). Droplet motion was analysed by single-particle tracking in sliding 60 s windows stepped by 30 s. Hydrodynamic diameters were estimated from drift-corrected trajectory mean-squared displacements using the Stokes−Einstein relation and summarised as medians of the per-track diameter of all accepted particles. Droplet count and integrated brightness were used to monitor changes in population and relative scattering intensity, respectively. Full imaging, tracking, analysis, and validation details are provided in Section S9.

2.6. Analysis of Fluorescence and Turbidity Traces

The first fluorescence cycle was excluded from quantitative analysis because it differed systematically from the later cycles. Cycles 2−4 were analysed independently, and transition temperatures are reported as mean ± SD. Cycle 2 is shown in the main figures; all cycles and the transition-temperature tables are provided in the Supporting Information (Section S5 for fluorescence and Section S7 for turbidity). Heating profiles were classified as suppressed, monotonic, or multistage. A fluorescence plateau was defined as a temperature interval in which the fluorescence changed more slowly than in the immediately preceding and subsequent stages. Characteristic temperatures were obtained by segmented linear regression and verified independently from derivative extrema and intensity thresholds.

Turbidity traces were plotted against temperature, and their transition and clearance temperatures were extracted using the same segmented-regression and derivative-based procedures. Full analysis details are provided in Section S5.

3. RESULTS

3.1. Nile Red Fluorescence

Nile Red fluorescence was recorded over four heating−cooling cycles for 12 conditions: citrate (pH 3), Tris (pH 7.4), and borate (pH 10), each containing 0−1.0 M NaCl (Figure 1). The first fluorescence cycle differed systematically from cycles 2−4 (Figure S9), whereas the turbidity traces were closely superimposable across successive cycles (Figure S11). Dye-only controls also showed a first-cycle difference (Figure S8a). The initial variation may therefore arise mainly from equilibration of the dye or its local environment, rather than from a major change in the aggregate population. Cycles 2−4 were reproducible, with standard deviations in transition temperatures typically ≤0.5 °C, and all quantitative values below refer to these cycles (Table S5).

The heating traces showed three different behaviours. (i) Multistage transitions occurred in citrate containing 0.5−1.0 M NaCl and in Tris containing 1.0 M NaCl; these traces showed an initial fluorescence rise, an extended plateau with a reduced slope, and a second rise at higher temperature. (ii) Monotonic transitions occurred under intermediate conditions, where fluorescence increased continuously without a resolved plateau. (iii) Borate containing 0−0.1 M NaCl showed no significant fluorescence increase, indicating no detectable formation of hydrophobic PNIPAM-rich domains. Characteristic temperatures for all conditions are listed in Table S5.

Within the citrate and Tris series, the onset temperature decreased linearly with NaCl concentration ($R^2 \approx 0.99$), with slopes of −14.8 ± 1.0 and −16.4 ± 1.0 °C M^{-1}, respectively (Figure 1c). The similar slopes indicate comparable salting-out sensitivity. At a fixed NaCl concentration, the onset was approximately 7−9 °C higher in Tris than in citrate. This pH-dependent shift corresponds to increasingly negative zeta potentials measured without added NaCl, from −1.9 ± 0.1 mV at pH 3 to −23.2 ± 2.2 mV at pH 7.4 and −39.4 ± 0.5 mV at pH 10, consistent with stronger electrostatic repulsion at higher pH.

At 1.0 M NaCl, lowering the pH generally broadened and flattened the intermediate fluorescence plateau (Figure 2). Additional measurements between pH 4.5 and 7.0 showed that the plateau width increased from 8.4 °C at pH 7.0 to 20.8 °C at pH 3.0, while its mean slope decreased from 4.4 to 2.3 a.u. $°C^{-1}$ (Table S6). The heating onset decreased with decreasing pH but levelled off below pH 4.5, reaching 26.1 ± 0.4 °C at pH 4.5 and 26.4 ± 0.0 °C at pH 3.

The two plateau boundaries responded differently to pH. Plateau entry closely tracked the onset, with an average offset of 7.0 ± 1.0 °C across the eight multistage conditions. By contrast, plateau exit was uncorrelated with onset. The plateau therefore broadened mainly through a downward shift of its entry temperature. The multistage pathway also had an upper pH boundary: borate containing 1.0 M NaCl showed a clear onset at 34.9 ± 0.4 °C, but its transition remained monotonic.

All non-suppressed conditions in the pH−salt screen showed thermal hysteresis, and the shape of the fluorescence recovery varied among conditions. On cooling, samples with a distinct multistage transition in the pH−salt screen exhibited an extended interval of slowly decreasing fluorescence before a sharp fluorescence decrease beginning at 28−31 °C, whereas other samples recovered progressively. The fluorescence hysteresis decreased with increasing NaCl concentration in both the citrate series (from 13.1 ± 0.2 °C without added NaCl to 6.2 ± 0.1 °C at 1.0 M NaCl) and the Tris series (from 11.4 ± 1.3 °C without added NaCl to 8.6 ± 0.5 °C at 1.0 M NaCl). However, the trend was reversed in borate, where the hysteresis increased from 0.7 ± 0.3 °C at 0.5 M NaCl to 9.3 ± 0.2 °C at 1.0 M NaCl.

3.2. Turbidimetry

Turbidity at 550 nm (A_{550}) is shown together with the Nile Red fluorescence in Figure 3. We found that A_{550} followed the same ordering across conditions as the fluorescence, with transition temperatures reproducible across cycles to within ± 0.3 °C in most cases (Figure 3 and Table S7). Unlike fluorescence, the first turbidity cycle generally overlapped with the later cycles, which supports the assignment of the first-cycle fluorescence change to dye equilibration rather than to a change in the aggregate population. Borate containing 0 or 0.1 M NaCl produced no measurable turbidity in any cycle, independently supporting their classification as suppressed.

During heating, turbidity onsets occurred systematically above the corresponding fluorescence onsets (Figure 4a), and the differences generally increased with NaCl concentration. This ordering is consistent with local dehydration preceding the formation of detectable light-scattering assemblies. In samples showing multistage fluorescence transitions, turbidity

Downloaded from pubs.acs.org/macmobx/article-pdf/doi/10.1021/acs.macromol.6c01188/6895939/ma-2026-011886.pdf by UNIV OF CAMBRIDGE user on 23 October 2026

https://doi.org/10.1021/acs.macromol.6c01188
Macromolecules XXXX, XXX, XXX−XXX

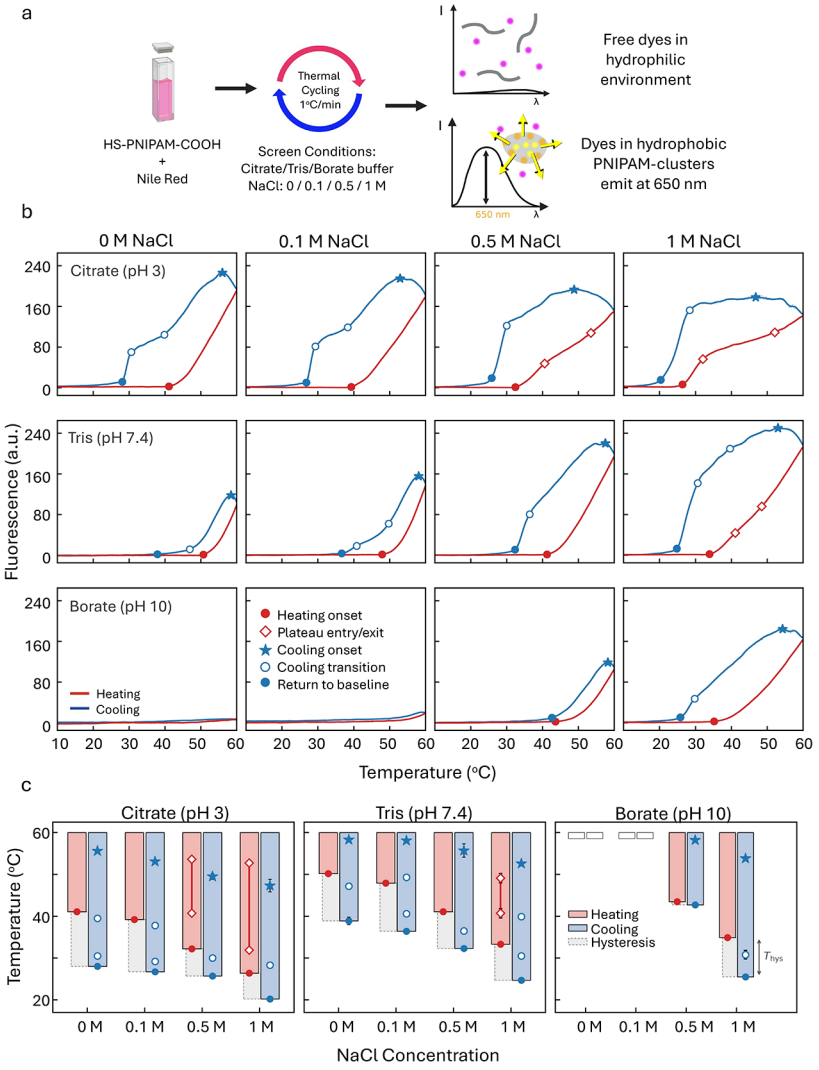


Figure 1. (a) Experimental workflow. Nile Red becomes strongly fluorescent after partitioning into hydrophobic PNIPAM-rich domains. (b) Nile Red fluorescence during cycle 2 in three buffers (pH measured at 25 °C; rows) and at four NaCl concentrations (columns). All thermal cycles are shown in Figure S9. (c) Characteristic temperatures extracted from cycles 2–4 (mean ± SD): red and blue bars span the heating and cooling branches, respectively, with symbols as in (b); the grey dashed box marks the hysteresis (T_{hys}) between the heating onset and the cooling return to baseline; open boxes mark suppressed conditions.

showed no resolved multistage rise. Instead, it continued to increase across the fluorescence plateau and approached saturation near the onset of the second fluorescence rise. In citrate containing 0.5 and 1.0 M NaCl, the absorbance reached maxima at 54.7 and 51.8 °C, respectively, close to the plateau exit, before decreasing by 3.3 and 3.2% by the end of heating.

The order of fluorescence and turbidity recovery during cooling also varied systematically (Figure 4b). In citrate, turbidity persisted 2.4–4.6 °C below the fluorescence-clearance temperature at every NaCl concentration. The offset was smaller in high-salt Tris and in borate at 0.5 M NaCl, whereas the two clearance temperatures coincided within experimental uncertainty in Tris at 0.1 M NaCl and borate at 1.0 M NaCl. In Tris without added NaCl, the order reversed, with turbidity returning to baseline before fluorescence. These smaller or reversed offsets at higher pH are consistent with charge facilitating aggregate disassembly relative to local rehydration, allowing larger scatterers to disassemble before smaller polymer-rich domains fully rehydrate under some highly charged, weakly screened conditions.

The turbidity hysteresis was larger than the fluorescence hysteresis by approximately 3–9 °C, except in Tris without added NaCl (Figure 4c). In citrate, the turbidity hysteresis also narrowed with added salt, from 18.8 ± 0.2 °C without added NaCl to 12.1 ± 0.2 °C at 1.0 M NaCl, whereas in Tris it remained near 14.8 °C between 0.1 and 1.0 M NaCl. Borate showed the opposite salt dependence: from 0.5 to 1.0 M NaCl, the turbidity hysteresis increased from 5.6 ± 1.1 to 15.8 ± 0.2 °C.

3.3. Dark-Field Microscopy Tracking of Mesoglobule Growth and Dissolution

Single-particle tracking via dark-field microscopy revealed different droplet-growth behaviour in the monotonic conditions C0 (citrate without added NaCl) and B1 (borate with 1.0 M NaCl), compared with the multistage condition C1 (citrate with

Downloaded from pubs.acs.org/mamobx/article-pdf/doi/10.1021/acs.macromol.6c01188/6895793939/ma-2026-011886.pdf by UNIV OF CAMBRIDGE user on 23 October 2026

https://doi.org/10.1021/acs.macromol.6c01188
Macromolecules XXXX, XXX, XXX–XXX

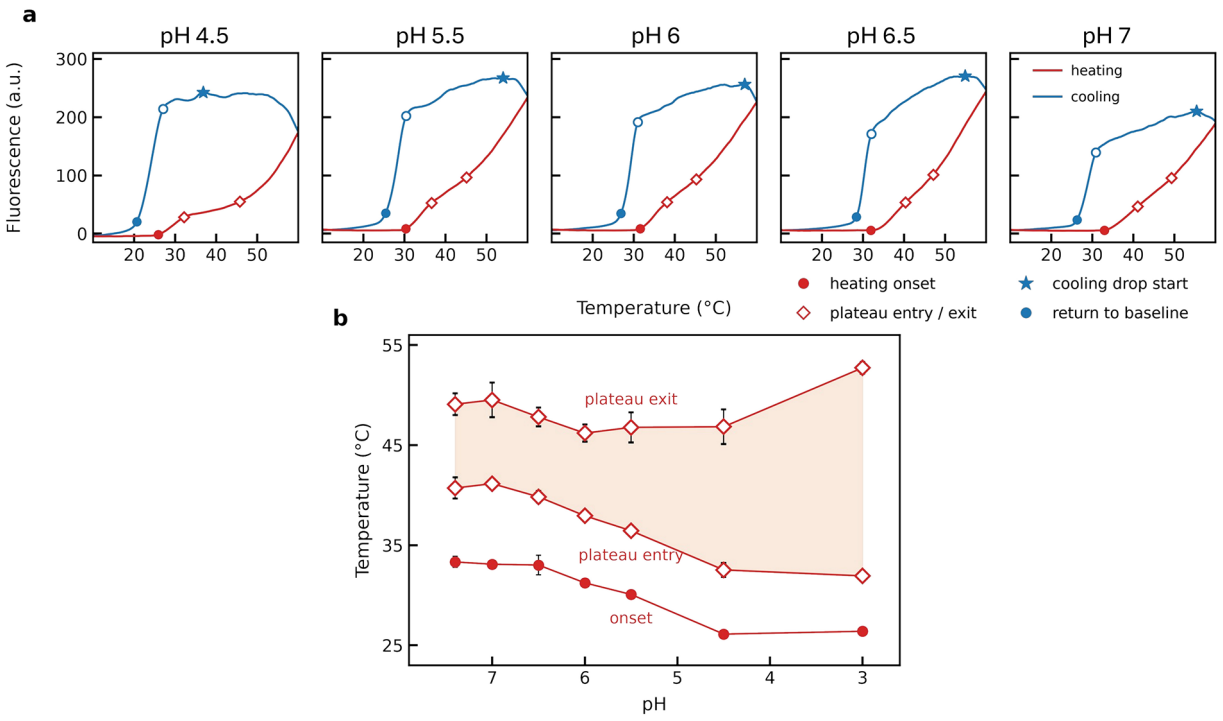


Figure 2. (a) Nile Red fluorescence for samples containing 1.0 M NaCl at pH 4.5−7.0 (cycle 2). (b) Onset, plateau-entry, and plateau-exit temperatures across pH 3−7.4 at 1.0 M NaCl. Characteristic temperatures are listed in Tables S5 and S6.

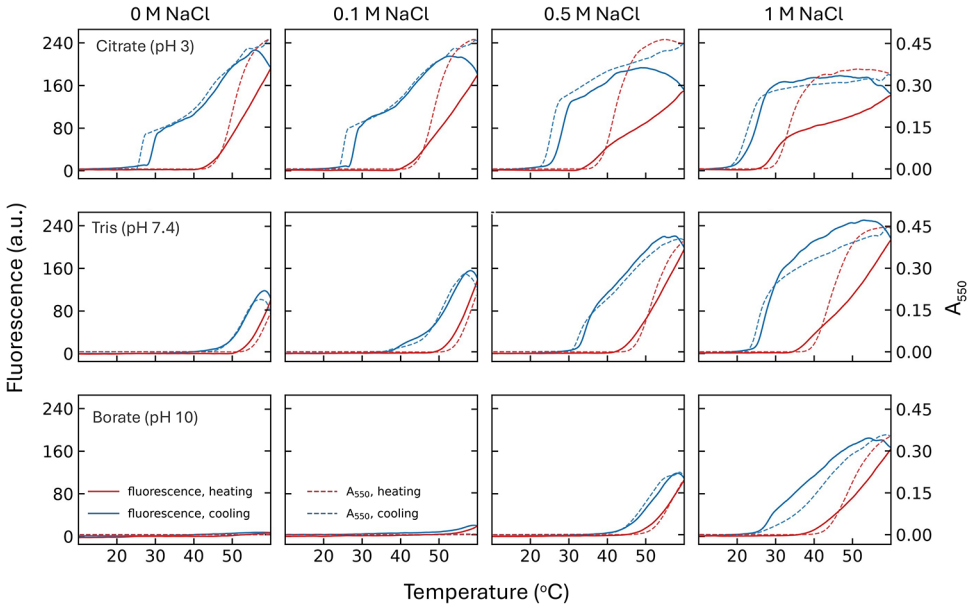


Figure 3. Baseline-corrected apparent absorbance at 550 nm (A_{550}, dashed lines) during heating and cooling for all buffer and NaCl conditions, overlaid with the corresponding Nile Red fluorescence traces (solid lines). Cycle 2 is shown; all cycles are given in Figure S11.

1.0 M NaCl). C0 and B1 showed continuous growth during every isothermal hold above the heating onset (Figure 5a,b), with larger temperature jumps generally producing greater size increases. Their size distributions shifted towards larger diameters rather than changing through loss of smaller droplets. In contrast, C1 showed initial continuous growth at 28 °C, followed by a growth-arrested stage approximately coinciding with the fluorescence plateau (Figure 5c). During this stage, droplets formed close to their final size within the first analysis window and remained nearly constant or decreased slightly during holds at 32−50 °C. Growth resumed only at 60 °C, during the second fluorescence rise, with the median diameter increasing by approximately 8%.

Droplet counts increased during holds slightly above the heating onset, consistent with continued nucleation or growth into the detection range, whereas larger temperature jumps

Downloaded from pubs.acs.org/macmobx/article-pdf/doi/10.1021/acs.macromol.6c01188/6895793939/ma-2026-011886.pdf by UNIV OF CAMBRIDGE user on 23 October 2026

https://doi.org/10.1021/acs.macromol.6c01188
Macromolecules XXXX, XXX, XXX−XXX

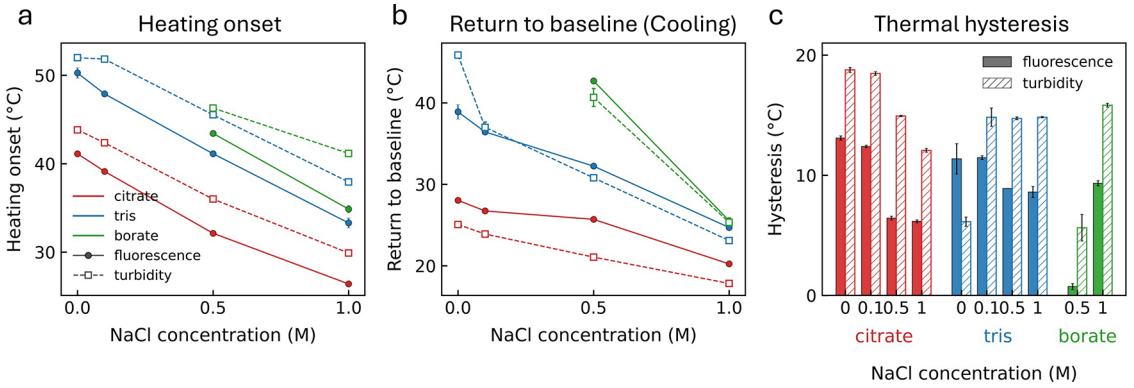


Figure 4. Comparison of fluorescence and turbidity transition temperatures (cycles 2−4, mean ± SD; Tables S5 and S7). (a) Heating onset, (b) return-to-baseline temperatures on cooling, and (c) thermal hysteresis as a function of NaCl concentration in each buffer.

produced an initial nucleation burst followed by a steady decline in droplet count. In C0 and B1, total scattered intensity decreased more slowly than droplet count, and the remaining droplets became brighter as they grew (Figure S20). During the C1 plateau holds, total scattered intensity and count decreased at similar rates while per-droplet brightness remained unchanged. Fusion between resolved droplets was rare across all conditions (Figure S23). These observations are consistent with sedimentation without concurrent growth during the C1 plateau holds and support growth in C0 and B1 through uptake of unresolved polymer species from the surrounding solution, potentially including sub-resolution clusters, rather than fusion between larger particles. Vertical scans at 60 °C showed sedimentation in both C1 and B1, with droplet count and total scattered intensity increasing from the bulk solution towards the substrate. The steeper gradients and lower bulk droplet count and scattered intensity in the multistage C1 sample indicated more pronounced sedimentation than in the monotonic B1 sample (Figure S19).

Cooling also distinguished the monotonic and multistage pathways. Following shallow cooling, both monotonic samples showed gradual droplet shrinkage (Figure 6a,b). For C0, cooling from 60 to 40 °C reduced the median diameter from 0.83 to 0.69 μm (−16%) over 15 min. For B1, cooling to 45 °C reduced the median diameter by 7%, whereas further cooling to 35 °C produced another 13% size decrease. Further cooling to 25 °C led to the disappearance of the C0 and B1 droplet populations within approximately 1−3 min. C1 again followed a distinct pathway (Figure 6c). Cooling from 60 to 40 °C left the median diameter nearly unchanged at approximately 1.00 μm. The gradual shrinkage in the monotonic samples was consistent with their progressive fluorescence decrease, whereas droplet persistence in C1 accompanied its extended cooling fluorescence plateau. After further cooling to 25 °C, the population remained stable for approximately 75 s before the count fell from 206 to 4 droplets per frame within approximately 30 s. This collapse was essentially population-wide, with > 90% of tracked droplets disappearing simultaneously.

3.4. Dynamic Light Scattering

Isothermal DLS correlation functions further supported the distinct dynamical regimes observed during heating (Figure S24). In the monotonic samples C0 and B1 at 50 °C, the correlation functions remained stretched and oscillatory and continued to evolve during the measurements, consistent with the sustained droplet growth observed by microscopy.

In contrast, C1 exhibited stage-dependent behaviour. Slightly above the transition onset, at 30 °C, stretched, time-dependent decays indicated a broad range of relaxation times and continuing evolution. Within the fluorescence plateau at 35−40 °C, the initially fluctuating correlation functions converged to reproducible, single-step decays that remained nearly unchanged throughout the remainder of the hold. This behaviour was consistent with the growth arrest observed by microscopy. Upon further heating to 50−60 °C, the correlations became stretched and oscillatory again, indicating renewed dynamics near and beyond the plateau boundary.

At 50 °C, DLS detected non-stationary dynamics despite the absence of measurable growth in the optically resolved droplets. This difference may arise because DLS is sensitive to sub-resolution rearrangements, polydispersity, and directed motion that do not necessarily produce a measurable change in the median size of the resolved droplets.

4. DISCUSSION

The combined measurements identify multistage, monotonic, and suppressed phase-separation pathways in heterotelechelic HS−PNIPAM−COOH as solution pH and NaCl concentration are varied. We propose that pathway selection reflects the balance among end-group ionisation, electrostatic screening, dehydration, and interfacial chain relaxation (Figure 7).

4.1. Coupled Roles of pH and NaCl in Pathway Selection

Increasing pH promotes ionisation of the terminal carboxyl and thiol groups, enhancing end-group hydration and electrostatic repulsion and delaying the earliest detectable fluorescence increase. The PNIPAM repeat units are not ionised across pH 3−10. In the extended 1.0 M NaCl series, the onset remained constant below pH 4.5 but increased primarily between pH 4.5 and 6.5, before levelling off again up to pH 7.4, consistent with deprotonation of the carboxyl terminus as the dominant pH-dependent contribution in this range.[23] At pH 10, thiol ionisation may contribute to the further onset increase and to the pronounced change in macroscopic association.[24] Under weak screening, end-group ionisation was associated with suppression of detectable interchain association, although intrachain collapse below the detection limit cannot be excluded. The borate

Downloaded from pubs.acs.org/macmobx/article-pdf/doi/10.1021/acs.macromol.6c01188/6895739/ma-2026-011886.pdf by UNIV OF CAMBRIDGE user on 23 October 2026

https://doi.org/10.1021/acs.macromol.6c01188
Macromolecules XXXX, XXX, XXX−XXX

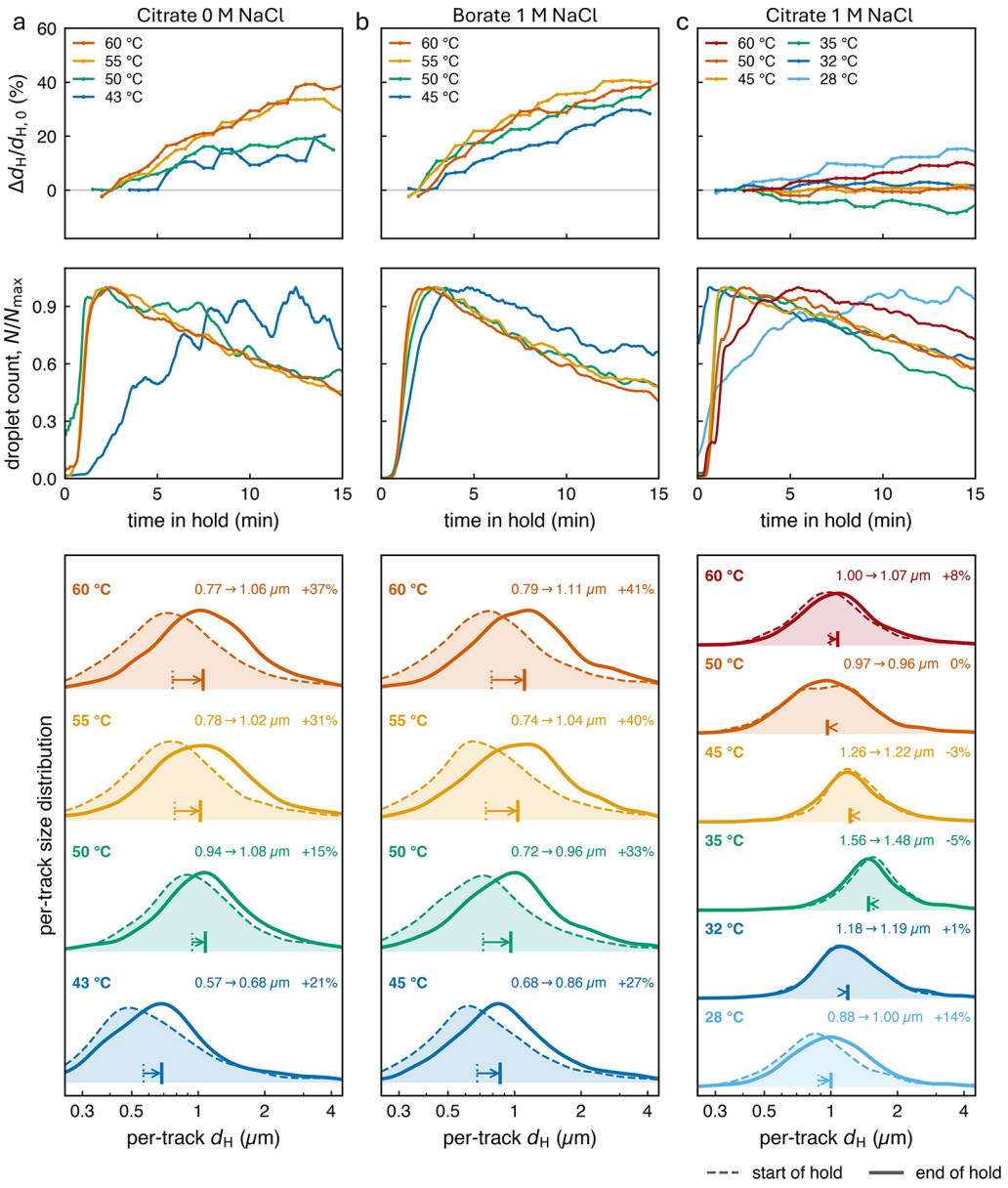


Figure 5. Evolution of PNIPAM mesoglobules during 15 min isothermal holds following heating jumps for (a) C0 (citrate without added NaCl), (b) B1 (borate + 1.0 M NaCl), and (c) C1 (citrate + 1.0 M NaCl); colour denotes the hold temperature. Top row: relative change in the median hydrodynamic diameter from the start of each hold, $\Delta d_H/d_{H,0}$. Middle row: droplet count per field of view normalised to the maximum reached during that hold, N/N_{max}. Bottom row: per-track size distributions pooled over the first three (dashed) and last three (solid) retained 60 s windows of each hold, spanning 120 s each. Absolute diameters and droplet counts are shown in Figure S21.

series also illustrates the role of NaCl screening, progressing from no detectable transition at 0−0.1 M NaCl, to partial aggregation at 0.5 M, and to strongly hysteretic aggregation at 1.0 M.

NaCl lowered the fluorescence onset with comparable slopes in the citrate and Tris series. This suggests salting-out of the PNIPAM backbone with comparable sensitivity under the two ionisation conditions.[13,14] The increasing separation between the fluorescence and turbidity onsets with higher NaCl concentration suggests that local dehydration and the formation of polymer-rich domains are more salt-sensitive than the emergence of detectable scattering assemblies. NaCl therefore shifts the initial collapse and association to lower temperatures. Subsequent coarsening may remain limited by particle encounters and interfacial rearrangement, as suggested by the mesoglobule-growth studies discussed above.[8,11]

Electrostatic screening alone, however, cannot explain pathway selection. Pronounced pH dependence persisted at 1.0 M NaCl, where the Debye screening length is approximately 0.3 nm: lowering the pH generally broadened and flattened the fluorescence plateau, whereas the borate response remained monotonic. This residual dependence suggests that local end-group hydration and interfacial mobility remain important even when long-range electrostatic interactions are strongly screened, although specific buffer effects cannot be excluded. Hydrated, ionised termini may maintain a softer and more mobile interface, favouring continuous growth once association becomes

https://doi.org/10.1021/acs.macromol.6c01188
Macromolecules XXXX, XXX, XXX−XXX

Downloaded from pubs.acs.org/mamobx/article-pdf/doi/10.1021/acs.macromol.6c01188/6895793/ma-2026-011886.pdf by UNIV OF CAMBRIDGE user on 23 October 2026

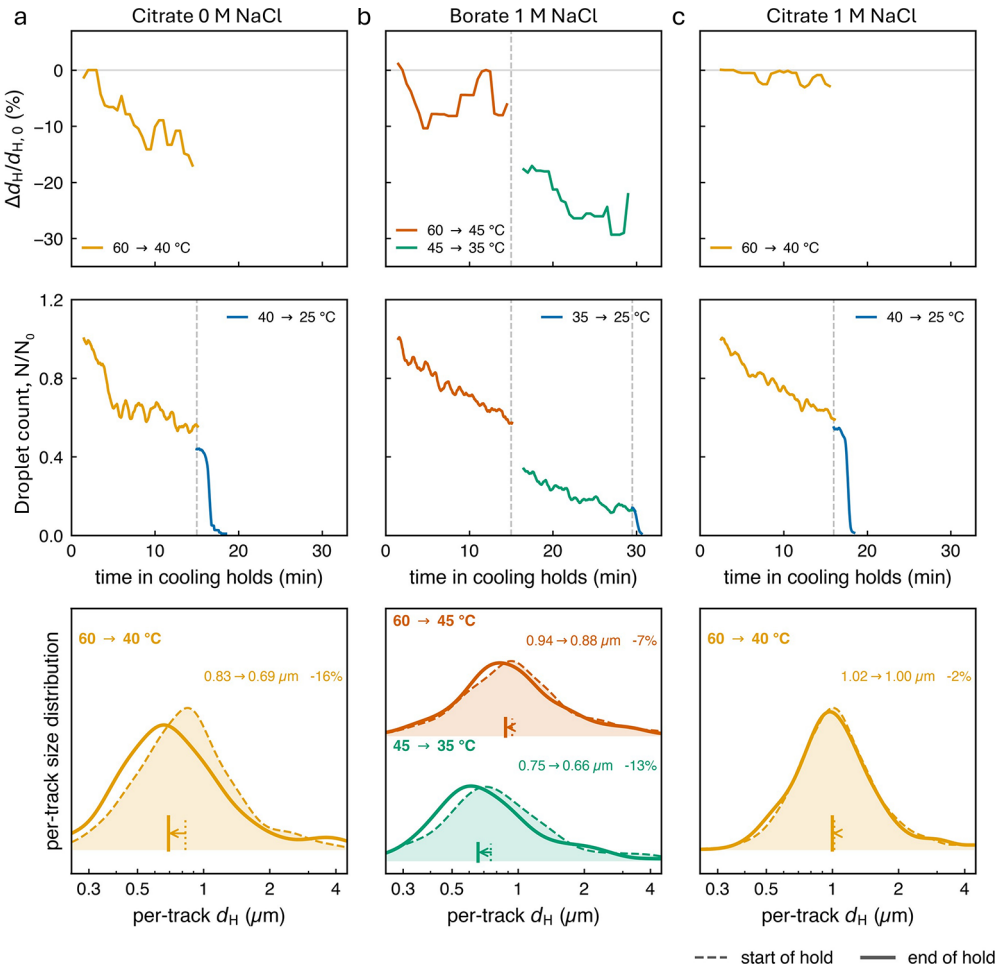


Figure 6. Evolution during the cooling protocol for (a) C0, (b) B1, and (c) C1. Successive holds are concatenated on a common axis of cumulative time in the cooling holds; dashed vertical lines mark the temperature steps, and colour denotes the temperature of each hold. Top row: relative change in the median hydrodynamic diameter from the start of the first cooling hold, $\Delta d_H/d_{H,0}$. Middle row: droplet count normalised to its value at the start of the first cooling hold, N/N_0, including the final quenches to 25 °C (blue), in which all three populations collapse within 1−3 min. Bottom row: per-track size distributions pooled over the first three (dashed) and last three (solid) retained 60 s windows of each cooling hold above 25 °C, spanning 120 s each. Sizes are not reported for the 25 °C quenches because the droplets disappear faster than a reliable estimate can be formed. Absolute diameters and droplet counts are shown in Figure S22.

possible. By contrast, protonated termini combined with strong NaCl-induced dehydration may promote rapid chain collapse and association, leading to interfacial densification and kinetic arrest. The transition from continuous to multistage profiles between 0 and 1.0 M NaCl at pH 7.4 (Figure 1) illustrates how increasing salt shifts the balance from sustained coarsening towards kinetically hindered, multistage growth.

4.2. Multistage Pathway: Proposed Kinetic Trapping by Interfacial Densification

C1 provides the clearest evidence that the multistage response represents a distinct aggregation pathway (Figure 7, Pathway I). During the fluorescence plateau, the median mesoglobule size remained nearly constant and the DLS correlations at 35−40 °C became stationary, whereas turbidity continued to increase. This combination is consistent with structural evolution without substantial particle growth.

We propose that low pH and high NaCl accelerate PNIPAM dehydration, causing chains to collapse rapidly into globules or small polymer-rich clusters. During collisions, chain relaxation may be too slow for complete interpenetration and fusion, producing loosely connected, fractal-like assemblies.[31] Scattering studies identified an analogous progression from transient fractal clusters to compact mesoglobules whose stiff surfaces limit further particle growth.[10,11,32] This behaviour is also compatible with topological repulsion between collapsed globules[33] and with the reported fluid-to-rigid transition of PNIPAM particles.[8] Continued dehydration may densify the outer regions and the interdomain contacts, arresting further coalescence while retaining water-filled interstitial regions.

This proposed structure could account for the different fluorescence and turbidity responses. Nile Red reports the local polarity of the dehydrated polymer-rich domains, so its fluorescence may plateau soon after these domains form. Turbidity, by contrast, remains sensitive to particle-scale density and refractive-index contrast; continued expulsion of interstitial water could thus increase turbidity without changing fluorescence or median particle size. The combined measurements are therefore consistent with progressive densification of porous, incompletely fused mesoglobules during the plateau

Downloaded from pubs.acs.org/macroabx/article-pdf/doi/10.1021/acs.macromol.6c01188/6895939/ma-2026-011886.pdf by UNIV OF CAMBRIDGE user on 23 October 2026

https://doi.org/10.1021/acs.macromol.6c01188
Macromolecules XXXX, XXX, XXX−XXX

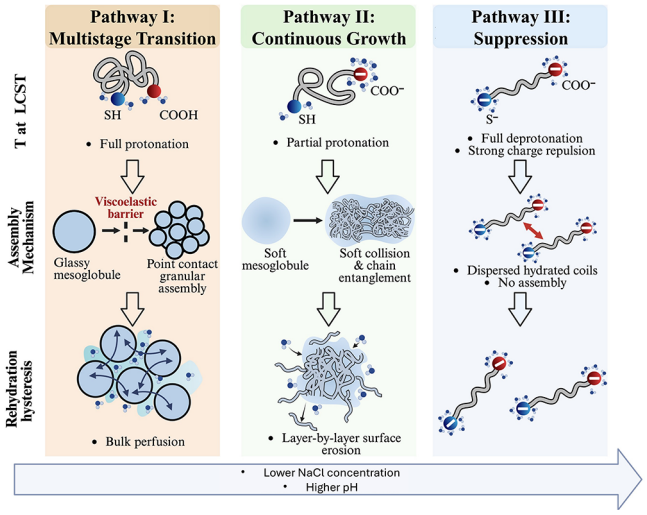


Figure 7. Proposed pH- and NaCl-dependent phase-separation pathways of HS−PNIPAM−COOH. In Pathway I (multistage, e.g., citrate with 1.0 M NaCl), rapid dehydration is proposed to create a densified, viscoelastic interface that arrests growth until further heating; dissolution during cooling is delayed and collective. In Pathway II (monotonic, e.g., citrate without added NaCl and borate with 1.0 M NaCl), mobile interfaces allow continuous growth from a reservoir of unresolved polymer species (potentially including sub-resolution clusters) and gradual chain release during cooling before final dissolution. In Pathway III (suppressed, e.g., borate with 0 or 0.1 M NaCl), strongly ionised, weakly screened chains do not form detectable mesoscopic assemblies. Schematic; not drawn to scale.

(Figure 7, Pathway I), although direct confirmation would require time-resolved SANS or SAXS. A plateau at a single emission wavelength is not unique evidence of constant hydration, because dye partitioning, spectral shifts, and optical attenuation can also affect the signal.

At higher temperature, the second fluorescence increase coincided with renewed microscopic growth and evolving DLS correlation functions, marking escape from the arrested state. A deeper thermal quench increases the thermodynamic driving force for polymer-rich contacts and may enable repeated encounters to overcome the barrier to interfacial rearrangement. The accompanying oscillatory DLS correlations may reflect directed motion,[34] while the turbidity maximum and subsequent decrease are consistent with sedimentation and loss of large particles from the measurement volume, as supported by the vertical scans at 60 °C (Figure S19).

The distinct cooling response further supports this pathway. C1 remained near sizes of 1.00 μm after cooling to 40 °C and persisted transiently at 25 °C before dissolving collectively (Section 3.3). Fluorescence returned to baseline before turbidity, consistent with local rehydration preceding complete particle disassembly. Such persistence is consistent with the established hysteresis of PNIPAM collapse and rehydration,[35] which has been associated with intrachain structures formed in the collapsed state[36] and with intersegment hydrogen bonds that act as transient physical cross-links within aggregates.[37] A densified interface could therefore permit water entry while restricting chain escape, allowing internal rehydration or swelling before the particle loses its integrity and dissolves collectively. We describe this mechanism tentatively as permeation-driven rehydration, by analogy with the swelling-dominated disintegration reported under strong osmotic driving forces.[12] The arrested plateau during heating and the delayed, collective dissolution during cooling may thus reflect the same structural feature: a densified interface that restricts both further coalescence and gradual chain release.

4.3. Monotonic Pathway: Reservoir-Fed Growth and Surface-Limited Rehydration

In C0 and B1, sustained increases in droplet size and brightness accompanied declining counts, while fusion between resolved droplets remained rare (Figures 5, S20, and S23). Together, these observations suggest continued uptake of polymer from the surrounding solution, potentially through coalescence with sub-resolution clusters. One possible contribution is Ostwald ripening, in which larger domains grow at the expense of smaller ones through the surrounding phase.[38,39] An alternative is the diffusion-limited coalescence of small mesoglobules observed by kinetic SANS.[11,32] The present measurements do not distinguish these contributions. Reservoir-fed growth is plausible when dehydration is relatively slow, as in C0 without added NaCl, or when hydrated, ionised termini maintain interfacial mobility, as in B1. The coupled evolution of fluorescence, turbidity, and particle size during heating is consistent with dehydration accompanying continued growth (Figure 7, Pathway II). This contrasts with C1, where droplet size and brightness remained nearly constant through the plateau while the resolved count and total intensity declined in parallel.

Cooling provides complementary evidence for continuous interfacial exchange. C0 and B1 droplets shrank gradually during shallow cooling, with the size distribution shifting towards smaller diameters. The gradual shrinkage in C0 and B1 is analogous to the gradual release of chains from mesoglobule surfaces reported under weak osmotic driving forces[12] and is therefore described tentatively as surface-limited rehydration.

The fluorescence−turbidity clearance sequence and offset also varied across conditions: fluorescence cleared first in C0, whereas the two clearances coincided within uncertainty in B1 (Table S7). The reversed ordering in salt-free Tris further shows that mesoscale structures can disassemble while smaller PNIPAM-rich regions remain partially dehydrated. This also supports the idea that sequential uptake of small PNIPAM clusters during heating may produce a compact, older interior surrounded by more recently incorporated and less strongly interpenetrated material, allowing the peripheral material to be released first during cooling. This internal hierarchy remains a working model rather than a directly resolved structure.

5. CONCLUSIONS

We used solvatochromic Nile Red fluorescence together with turbidimetry, DLS, and dark-field imaging to examine how end-group ionisation and NaCl concentration regulate the phase separation of heterotelechelic HS−PNIPAM−COOH ($M_n \approx 6$ kDa). Across different combinations of pH and salt, three distinct behaviours were identified: (i) a multistage transition with long-lived mesoglobule intermediates under weakly ionised, high-salt conditions, (ii) monotonic transitions under intermediate conditions, and (iii) suppressed transitions under strongly ionised and weakly screened conditions. The distinct cooling behaviours of the monotonic and multistage regimes provide evidence that the resulting high-temperature states differ in their organisation and persistence. We propose that pH

Downloaded from pubs.acs.org/macmobx/article-pdf/doi/10.1021/acs.macromol.6c01188/6895739/ma-2026-011886.pdf by UNIV OF CAMBRIDGE user on 23 October 2026

https://doi.org/10.1021/acs.macromol.6c01188
Macromolecules XXXX, XXX, XXX−XXX

sets the baseline hydration and interfacial mobility of PNIPAM-rich domains through end-group ionisation, while NaCl both screens residual electrostatic repulsion and promotes dehydration. When dehydration outpaces interfacial relaxation, mesoglobules may become kinetically trapped by a viscoelastic barrier to coalescence.

These findings suggest several directions for future work. Scattering techniques with structural resolution (particularly time-resolved SANS or SAXS) could directly test the proposed interfacial densification mechanism by probing mesoglobule radial density profiles under different pH−salt conditions. Extending the approach to PNIPAM of higher molecular weight, different architectures, or alternative ionisable end groups would clarify the generality of the pathway-selection framework. More broadly, the ability to select among kinetically distinct pathways using only pH and salt concentration should prove useful for applications in which mesoglobule lifetime is a critical design parameter.

■ ASSOCIATED CONTENT

Data Availability Statement

Data supporting this study are provided in the article and its Supporting Information.

Supporting Information

The Supporting Information is available free of charge at https://pubs.acs.org/doi/10.1021/acs.macromol.6c01188.

Polymer molecular-weight characterisation by SEC and NMR, concentration-dependent cloud point in pure water, and effect of purification by precipitation (S1); TCEP controls (S2); buffer pH−temperature profiles and MOPS comparison (S3); Nile Red concentration and dye-only controls (S4); all fluorescence thermal cycles, transition-temperature analysis, and tabulated characteristic temperatures (S5); the extended pH series at 1.0 M NaCl (S6); all turbidity thermal cycles, turbidity transition temperatures, and sample photographs (S7); differential scanning calorimetry (S8); optical microscopy and single-particle-tracking methods, validation, vertical sedimentation profile, and Movies S1−S6 (S9); and DLS correlation functions with buffer-only controls (S10) (PDF)

Tracking_fresh_c0_50°C (MP4)

Tracking_fresh_b1_50°C (MP4)

Tracking_fresh_c1_35°C (MP4)

Tracking_fresh_c1_50°C (MP4)

Tracking_fresh_c1_60°C (MP4)

Scan_c1_vs_b1_diffusing (MP4)

■ AUTHOR INFORMATION

Corresponding Authors

Ulrich F. Keyser − *Cavendish Laboratory, Department of Physics, University of Cambridge, Cambridge CB3 0HE, U.K.;* Email: ufk20@cam.ac.uk

Jeremy J. Baumberg − *NanoPhotonics Centre, Cavendish Laboratory, Department of Physics, University of Cambridge, Cambridge CB3 0HE, U.K.;* orcid.org/0000-0002-9606-9488; Email: jjb12@cam.ac.uk

Authors

Yuhang Zhang − *NanoPhotonics Centre, Cavendish Laboratory, Department of Physics, University of Cambridge, Cambridge CB3 0HE, U.K.*

Tianlai Xia − *School of Chemistry, University of Birmingham, Edgbaston, Birmingham B15 2TT, U.K.;* orcid.org/0000-0002-4391-0296

Jin Qin − *NanoPhotonics Centre, Cavendish Laboratory, Department of Physics, University of Cambridge, Cambridge CB3 0HE, U.K.*

Thieme T. Schmidt − *NanoPhotonics Centre, Cavendish Laboratory, Department of Physics, University of Cambridge, Cambridge CB3 0HE, U.K.;* orcid.org/0000-0002-6802-3036

Rachel K. O'Reilly − *School of Chemistry, University of Birmingham, Edgbaston, Birmingham B15 2TT, U.K.;* orcid.org/0000-0002-1043-7172

Complete contact information is available at: https://pubs.acs.org/doi/10.1021/acs.macromol.6c01188

Author Contributions

Y.Z., T.T.S., and J.J.B. conceived and designed the experiments. Y.Z. performed the experiments with support from T.T.S. and carried out the data analysis. Y.Z., J.J.B., and U.F.K. developed the mechanistic interpretation. T.X. and R.K.O. assisted with the chemical characterisation of the polymer, and J.Q. assisted with setting up the microscopy imaging experiments. All authors contributed to writing, reviewing, and editing the manuscript.

Notes

The authors declare no competing financial interest.

■ ACKNOWLEDGMENTS

The authors acknowledge financial support from the European Research Council (ERC) under the Horizon 2020 research and innovation programme, grant agreements PICOFORCE (No. 883703), and from the EPSRC (Cambridge NanoDTC EP/L015978/1, EP/L027151/1, EP/X037770/1, UKRI1255, and UKRI3173). T.T.S. was supported by the Data-Piets Fonds. Y.Z. was supported by the Cambridge Trust and the George and Lillian Schiff Studentship. Claude was used for data analysis and paper editing.

■ REFERENCES

(1) Halperin, A.; Kröger, M.; Winnik, F. M. Poly(N-isopropylacrylamide) Phase Diagrams: Fifty Years of Research. *Angew. Chem., Int. Ed.* **2015**, *54*, 15342−15367.

(2) Wu, C.; Zhou, S. Laser Light Scattering Study of the Phase Transition of Poly(N-isopropylacrylamide) in Water. 1. Single Chain. *Macromolecules* **1995**, *28*, 8381−8387.

(3) Aseyev, V.; Hietala, S.; Laukkanen, A.; Nuopponen, M.; Confortini, O.; Du Prez, F. E.; Tenhu, H. Mesoglobules of Thermoresponsive Polymers in Dilute Aqueous Solutions above the LCST. *Polymer* **2005**, *46*, 7118−7131.

(4) Chan, K.; Pelton, R.; Zhang, J. On the Formation of Colloidally Dispersed Phase-Separated Poly(N-isopropylacrylamide). *Langmuir* **1999**, *15*, 4018−4020.

(5) Gorelov, A. V.; Du Chesne, A.; Dawson, K. A. Phase Separation in Dilute Solutions of Poly(N-isopropylacrylamide). *Phys. A* **1997**, *240*, 443−452.

Downloaded from pubs.acs.org/mamobx/article-pdf/doi/10.1021/acs.macromol.6c01188/6895939/ma-2026-011886.pdf by UNIV OF CAMBRIDGE user on 23 October 2026

(6) Haladjova, E.; Toncheva-Moncheva, N.; Apostolova, M. D.; Trzebicka, B.; Dworak, A.; Petrov, P.; Dimitrov, I.; Rangelov, S.; Tsvetanov, C. B. Polymeric Nanoparticle Engineering: From Temperature-Responsive Polymer Mesoglobules to Gene Delivery Systems. *Biomacromolecules* **2014**, *15*, 4377−4395.
(7) Ji, D.; Liu, J.; Zhao, J.; Li, M.; Rho, Y.; Shin, H.; Han, T. H.; Bae, J. Sustainable 3D Printing by Reversible Salting-Out Effects with Aqueous Salt Solutions. *Nat. Commun.* **2024**, *15*, 3925.
(8) Kujawa, P.; Aseyev, V.; Tenhu, H.; Winnik, F. M. Temperature-Sensitive Properties of Poly(N-isopropylacrylamide) Mesoglobules Formed in Dilute Aqueous Solutions Heated above Their Demixing Point. *Macromolecules* **2006**, *39*, 7686−7693.
(9) Papadakis, C. M.; Niebuur, B.-J.; Schulte, A. Thermoresponsive Polymers under Pressure with a Focus on Poly(N-isopropylacrylamide) (PNIPAM). *Langmuir* **2024**, *40*, 1−20.
(10) Niebuur, B.-J.; Pipich, V.; Appavou, M.-S.; Mullapudi, D.; Nieth, A.; Rende, E.; Schulte, A.; Papadakis, C. M. PNIPAM Mesoglobules in Dependence on Pressure. *Langmuir* **2024**, *40*, 22314−22323.
(11) Niebuur, B.-J.; Chiappisi, L.; Jung, F.; Zhang, X.; Schulte, A.; Papadakis, C. M. Kinetics of Mesoglobule Formation and Growth in Aqueous Poly(N-isopropylacrylamide) Solutions: Pressure Jumps at Low and at High Pressure. *Macromolecules* **2019**, *52*, 6416−6427.
(12) Niebuur, B.-J.; Chiappisi, L.; Jung, F. A.; Zhang, X.; Schulte, A.; Papadakis, C. M. Nanoscale Disintegration Kinetics of Mesoglobules in Aqueous Poly(N-isopropylacrylamide) Solutions Revealed by Small-Angle Neutron Scattering and Pressure Jumps. *Nanoscale* **2021**, *13*, 13421−13426.
(13) Burba, C. M.; Carter, S. M.; Meyer, K. J.; Rice, C. V. Salt Effects on Poly(N-isopropylacrylamide) Phase Transition Thermodynamics from NMR Spectroscopy. *J. Phys. Chem. B* **2008**, *112*, 10399−10404.
(14) Zhang, Y.; Furyk, S.; Sagle, L. B.; Cho, Y.; Bergbreiter, D. E.; Cremer, P. S. Effects of Hofmeister Anions on the LCST of PNIPAM as a Function of Molecular Weight. *J. Phys. Chem. C* **2007**, *111*, 8916−8924.
(15) Furyk, S.; Zhang, Y.; Ortiz-Acosta, D.; Cremer, P. S.; Bergbreiter, D. E. Effects of End Group Polarity and Molecular Weight on the Lower Critical Solution Temperature of Poly(N-isopropylacrylamide). *J. Polym. Sci., Part A: Polym. Chem.* **2006**, *44*, 1492−1501.
(16) Xia, Y.; Burke, N. A. D.; Stöver, H. D. H. End Group Effect on the Thermal Response of Narrow-Disperse Poly(N-isopropylacrylamide) Prepared by Atom Transfer Radical Polymerization. *Macromolecules* **2006**, *39*, 2275−2283.
(17) Qiu, X. P.; Koga, T.; Tanaka, F.; Winnik, F. M. New Insights into the Effects of Molecular Weight and End Group on the Temperature-Induced Phase Transition of Poly(N-isopropylacrylamide) in Water. *Sci. China: Chem.* **2013**, *56*, 56−64.
(18) Sharker, K. K.; Takeshima, S.; Toyama, Y.; Ida, S.; Kanaoka, S.; Yusa, S.-I. pH- and Thermo-Responsive Behavior of PNIPAM Star Containing Terminal Carboxy Groups in Aqueous Solutions. *Polymer* **2020**, *203*, 122735.
(19) Collins, K. D. Ions from the Hofmeister Series and Osmolytes: Effects on Proteins in Solution and in the Crystallization Process. *Methods* **2004**, *34*, 300−311.
(20) Weng, Y.; Ding, Y.; Zhang, G. Microcalorimetric Investigation on the Lower Critical Solution Temperature Behavior of N-Isopropycrylamide-co-Acrylic Acid Copolymer in Aqueous Solution. *J. Phys. Chem. B* **2006**, *110*, 11813−11817.
(21) Yin, X.; Hoffman, A. S.; Stayton, P. S. Poly(N-isopropylacrylamide-co-propylacrylic acid) Copolymers That Respond Sharply to Temperature and pH. *Biomacromolecules* **2006**, *7*, 1381−1385.
(22) Locatelli-Champagne, C.; Cloitre, M. Monitoring Mesoglobules Formation in PNIPAm Solutions Using Nile Red Solvatochromism. *Colloid Polym. Sci.* **2013**, *291*, 2911−2916.
(23) Škvarla, J.; Raya, R. K.; Uchman, M.; Zedník, J.; Procházka, K.; Garamus, V. M.; Meristoudi, A.; Pispas, S.; Štěpánek, M. Thermoresponsive Behavior of Poly(N-isopropylacrylamide)s with Dodecyl and Carboxyl Terminal Groups in Aqueous Solution: pH-Dependent Cloud Point Temperature. *Colloid Polym. Sci.* **2017**, *295*, 1343−1349.
(24) Beaupre, D. M.; Weiss, R. G. Thiol- and Disulfide-Based Stimulus-Responsive Soft Materials and Self-Assembling Systems. *Molecules* **2021**, *26*, 3332.
(25) Getz, E. B.; Xiao, M.; Chakrabarty, T.; Cooke, R.; Selvin, P. R. A Comparison between the Sulfhydryl Reductants Tris(2-carboxyethyl)-phosphine and Dithiothreitol for Use in Protein Biochemistry. *Anal. Biochem.* **1999**, *273*, 73−80.
(26) Visser, C. C.; Voorwinden, L. H.; Harders, L. R.; Eloualid, M.; van Bloois, L.; Crommelin, D. J. A.; Danhof, M.; de Boer, A. G. Coupling of Metal Containing Homing Devices to Liposomes via a Maleimide Linker: Use of TCEP to Stabilize Thiol-Groups without Scavenging Metals. *J. Drug Target.* **2004**, *12*, 569−573.
(27) Bruce, E. E.; Bui, P. T.; Rogers, B. A.; Cremer, P. S.; van der Vegt, N. F. A. Nonadditive Ion Effects Drive Both Collapse and Swelling of Thermoresponsive Polymers in Water. *J. Am. Chem. Soc.* **2019**, *141*, 6609−6616.
(28) Bruce, E. E.; Bui, P. T.; Rogers, B. A.; Cremer, P. S.; van der Vegt, N. F. A. Addition to "Nonadditive Ion Effects Drive Both Collapse and Swelling of Thermoresponsive Polymers in Water". *J. Am. Chem. Soc.* **2021**, *143*, 2456.
(29) Yan, X.; Chu, Y.; Liu, B.; Ru, G.; Di, Y.; Feng, J. Dynamic Mechanism of Halide Salts on the Phase Transition of Protein Models, Poly(N-isopropylacrylamide) and Poly(N,N-diethylacrylamide). *Phys. Chem. Chem. Phys.* **2020**, *22*, 12644−12650.
(30) Bischofberger, I.; Trappe, V. New Aspects in the Phase Behaviour of Poly-N-isopropyl Acrylamide: Systematic Temperature Dependent Shrinking of PNiPAM Assemblies Well beyond the LCST. *Sci. Rep.* **2015**, *5*, 15520.
(31) Tanaka, H. Viscoelastic Phase Separation. *J. Phys.: Condens. Matter* **2000**, *12*, R207−R264.
(32) Niebuur, B.-J.; Chiappisi, L.; Zhang, X.; Jung, F.; Schulte, A.; Papadakis, C. M. Formation and Growth of Mesoglobules in Aqueous Poly(N-isopropylacrylamide) Solutions Revealed with Kinetic Small-Angle Neutron Scattering and Fast Pressure Jumps. *ACS Macro Lett.* **2018**, *7*, 1155−1160.
(33) Chuang, J.; Grosberg, A. Y.; Tanaka, T. Topological Repulsion between Polymer Globules. *J. Chem. Phys.* **2000**, *112*, 6434−6442.
(34) López-Molina, J.; Moncho-Jordá, A.; Tirado-Miranda, M. Measuring Absolute Velocities from Nonequilibrium Oscillations via Single-Detector 3D Dynamic Light Scattering. *Phys. Rev. Lett.* **2024**, *133*, 198202.
(35) Van Durme, K.; Van Assche, G.; Van Mele, B. Kinetics of Demixing and Remixing in Poly(N-isopropylacrylamide)/Water Studied by Modulated Temperature DSC. *Macromolecules* **2004**, *37*, 9596−9605.
(36) Wang, X.; Qiu, X.; Wu, C. Comparison of the Coil-to-Globule and the Globule-to-Coil Transitions of a Single Poly(N-isopropylacrylamide) Homopolymer Chain in Water. *Macromolecules* **1998**, *31*, 2972−2976.
(37) Cheng, H.; Shen, L.; Wu, C. LLS and FTIR Studies on the Hysteresis in Association and Dissociation of Poly(N-isopropylacrylamide) Chains in Water. *Macromolecules* **2006**, *39*, 2325−2329.
(38) Lifshitz, I. M.; Slyozov, V. V. The Kinetics of Precipitation from Supersaturated Solid Solutions. *J. Phys. Chem. Solids* **1961**, *19*, 35−50.
(39) Wagner, C. Theorie der Alterung von Niederschlägen durch Umlösen (Ostwald-Reifung). *Z. Elektrochem. Ber. Bunsenges. Phys. Chem.* **1961**, *65*, 581−591.

Downloaded from pubs.acs.org/macmobx/article-pdf/doi/10.1021/acs.macromol.6c01188/6895739/ma-2026-011886.pdf by UNIV OF CAMBRIDGE user on 23 October 2026